Astronomy & Astrophysics manuscript no. WR118˙v2˙9.hyper8652
September 23, 2009

LETTER TO THE EDITOR

VLTI/AMBER unveils a possible dusty pinwheel nebula in WR118.⋆

F. Millour[1], T. Driebe[1], O. Chesneau[2], J. H. Groh[1], K.-H. Hofmann[1],
K.. Murakawa[1], K. Ohnaka[1], D. Schertl[1], and G. Weigelt[1]

[1] Max-Planck-Institut für Radioastronomie, Auf dem Hügel 69, D-53121 Bonn, Germany,
e-mail: fmillour@mpifr-bonn.mpg.de
[2] Observatoire de la Côte d'Azur/CNRS, UMR 6525 H. Fizeau, Univ. Nice Sophia Antipolis, Avenue Copernic, 06130 Grasse, France

Version:September 23, 2009

ABSTRACT

Context. Most Wolf-Rayet stars (WR) of WC9 sub-type exhibit a dusty circumstellar envelope, but it is still a matter of debate how dust can form in their harsh environment. In a few cases, a pinwheel-like structure of the dusty envelope has been detected. Therefore, it has been suggested that dust formation in all dusty WR stars might be linked to colliding winds in a binary system.
Aims. We probed the innermost region of the circumstellar dust shell of the deeply embedded WR star WR 118.
Methods. We carried out spectro-interferometric observations using the AMBER instrument of ESO's Very Large Telescope Interferometer in low-spectral resolution mode ($R = 35$). The K-band observations were obtained with three 1.8 m telescopes spanning projected baselines between 9.2 and 40.1 m.
Results. At high spatial frequencies, the AMBER visibilities exhibit a prominent lobe, indicating that the envelope contains one or several zones with a large local intensity gradient. The strong closure phase signal clearly shows that the circumstellar envelope of WR 118 can only be described by an asymmetric intensity distribution. We show that a pinwheel nebula seen at low inclination is consistent with the AMBER data. Its size was determined to be 13.9 ± 1.1 mas.
Conclusions. WR 118 possibly harbors a pinwheel nebula, which suggests a binary nature of the system. According to our best model, the period of the system would be ≈ 60 days (for $d = 3$ kpc), making WR 118 the shortest-period pinwheel nebula known so far.

Key words. Stars: individual: WR 118, Stars: Wolf-Rayet, Stars: winds, outflows, Stars: circumstellar matter, Techniques: interferometric, Techniques: spectroscopic

1. Introduction

Since the work of Allen et al. (1972), infrared photometric studies of Wolf-Rayet (WR) stars have shown that many late-type WC stars have dust characteristics in addition to their typical free-free wind emission. For instance, Williams et al. (1987) showed that 85% of the WC9 stars and 50% of the WC8 stars are surrounded by heated ($T \sim 1300$ K) circumstellar amorphous carbon dust (see also Chiar et al. 2002). WR dust makers are rare but remarkable in terms of their absolute dust-formation rate, which can be as high as $\dot{M} = 10^{-6}\, M_{\odot}\mathrm{yr}^{-1}$.

Among the strongest infrared WR sources, some show a distinct periodic variability. Variable dust producers appear to be eccentric binary systems (WR+OB) where episodic dust formation coincides with periastron passage (see, e.g., Williams & van der Hucht 1992). Although our knowledge of dusty WR stars has considerably increased in the recent past, we are still far from a complete understanding of how dust can form in the hostile environment of these hot stars.

Using aperture-masking interferometry with the Keck telescope, it has been discovered that two supposedly single WRs with large IR excess, WR 104 and WR 98a, are close binary systems whose dust distribution is tracing the orbital motion of the binary components and forming a pattern which has been called "pinwheel" nebulae (Tuthill et al. 1999; Monnier et al. 1999, 2007). Recently, the number of WR stars and, in particular, dusty WCs discovered has considerably increased, especially in some open clusters towards the galatic center (van der Hucht 2006; Crowther et al. 2006; Tuthill et al. 2006). Among them, two new pinwheel nebulae were discovered in the Quintuplet cluster (Tuthill et al. 2006).

Binarity and wind clumping are currently the two best mechanisms to form dust in the circumstellar environment of WR stars. Observationally, distinguishing between these two cases is a challenging task. Direct spectroscopic evidence for a binary companion is difficult to reveal (Williams & van der Hucht 2000), but infrared long-baseline interferometry with its spatial capability offers a unique chance to resolve a central binary star and to determine the spatial distribution of dust created in the circumstellar environment of dust-enshrouded WR stars.

Recently, the dust shell of the persistent dust-maker WR 118 (spectral type WC9), the third-brightest WR star in the K band ($K = 3.65^{\mathrm{m}}$), could be resolved with speckle interferometry by Yudin et al. (2001) and Monnier et al. (2007). The radiative transfer modeling of Yudin et al. (2001) showed that grains can grow to sizes up to $\sim$0.6 μm. They also found that the inner dust-shell rim diameter of WR 118 is $r_{\mathrm{in}} = 17$ mas, temperature of the carbon-rich dust at the inner dust-shell boundary is 1750 ± 100 K, and dust formation rate is of the order of $10^{-7} M_{\odot}\mathrm{yr}^{-1}$. Using the Keck telescope, the aperture-masking observations of Monnier et al. (2007) confirmed the results of

⋆ The observations presented in this paper were obtained with the AMBER instrument of ESO's Very Large Telescope Interferometer (VLTI) as part of the Guaranteed Time Programme 079.D-0359(A) (PI: T. Driebe).

Yudin et al. (2001) by measuring a Gaussian FWHM of 23 mas at 2.3μm.

Here, we present the first infrared long-baseline interferometric observations of WR 118 obtained with AMBER, the near-infrared beam-combiner instrument (Petrov et al. 2007) of ESO's Very Large Telescope Interferometer (VLTI), giving access to spatial resolution ($\approx$ 10 mas) five times better than before. This allowed us to investigate the geometry of the innermost circumstellar dust shell of WR 118.

2. Observations and data processing

WR 118 was observed during three nights with AMBER in low spectral resolution mode (R = 35) in the J, H, and K bands. The telescope configuration used was E0-G0-H0 (linear array with baseline lengths of 16/32/48 m). Each measurement consists of 5000 frames with an exposure time of 100 ms. We reduced the data with version 2.2 of the AMBER software package `amdlib` (Tatulli et al. 2007)[1]. Following previous AMBER data reduction experience (e.g., Weigelt et al. 2007), we kept 20% of the frames with the highest fringe signal-to-noise ratio and discarded frames with an optical-path difference offset larger than 10 μm. Due to limitations related to the weather conditions and the extreme reddening of the object, the quality of the J- and H-band data turned out to be too low for a scientific analysis and were discarded. Thus, this paper discusses only the K-band (1.95 – 2.35μm) observations of WR 118. Also, we could only extract visibilities from the shortest baseline out of the 2007 dataset. An overview of the AMBER observations is given in Table 1, and the corresponding UV coverage is shown in the upper inset of Fig. 1.

object					
Date	Time [UTC]	Name	B_p [m]	PA [°]	seeing [″]
2007-10-08	02:18:53	WR 118	9.2	74.3	0.61
2008-03-28	08:43:43	WR 118	13.4-40.2	61.7	0.83
2008-03-31	06:51:05	WR 118	9.6-28.8	42.6	0.73
2008-03-31	07:09:33	WR 118	10.3-32.0	47.6	0.86
calibrators					
Date	Time [UTC]	HD number	UD [mas]	spectral type	seeing [″]
2007-10-08	01:07:58	175583	1.02 ± 0.01	K2III	0.66
2008-03-28	09:33:52	175583	1.02 ± 0.01	K2III	0.60
2008-03-31	07:42:46	175583	1.02 ± 0.01	K2III	0.81
2008-03-31	08:20:04	165524	1.11 ± 0.01	K3III	0.80

Table 1. Log of the AMBER observations of WR 118 (top) and the corresponding calibrators (bottom). B_p gives the range of projected baselines, and PA denotes the position angle of the observation. The calibrators' uniform-disk diameters were taken from Richichi et al. (2005) and the spectral types are from Simbad (`http://simbad.u-strasbg.fr`).

The calibrated AMBER visibilities and closure phases of WR 118 are shown in Fig. 1 as a function of spatial frequency q. The figure reveals a visibility decrease up to q = 60, followed by a "bump" around q = 80. This visibility shape is characteristic for an object intensity distribution that contains sharp edges. Examples of such intensity distributions are, e.g., a uniform disk or a ring-like intensity distribution. In addition, the AMBER data clearly show non-zero, non-180° closure phases, indicating that the circumstellar envelope deviates from a point-symmetric configuration. Therefore, from this qualitative analysis of the AMBER data, we can clearly rule out any centro-symmetric shape of the object; i.e., the circumstellar shell cannot be described by a simple circular or even elliptical envelope, as was done, for instance, in Yudin et al. (2001).

[1] provided by the Jean-Marie Mariotti Center, `http://www.jmmc.fr`

3. Modeling

3.1. Simple geometrical models

To interpret the AMBER data, we first tried to fit them with simple two-component geometrical models: one resolved component (Gaussian disk, uniform disk, or ring) to account for the overall visibility decrease towards larger spatial frequencies, and one spatially off-set component (resolved or not) to account for asymmetry, mainly probed by the non-zero closure phase. We assumed that the object's intensity distribution is not wavelength-dependent in order to take advantage of the larger UV coverage. We performed a global optimization of the fit by using a simulated annealing algorithm, complemented with standard gradient descent (see Millour et al. 2009, for a first use of these algorithms).

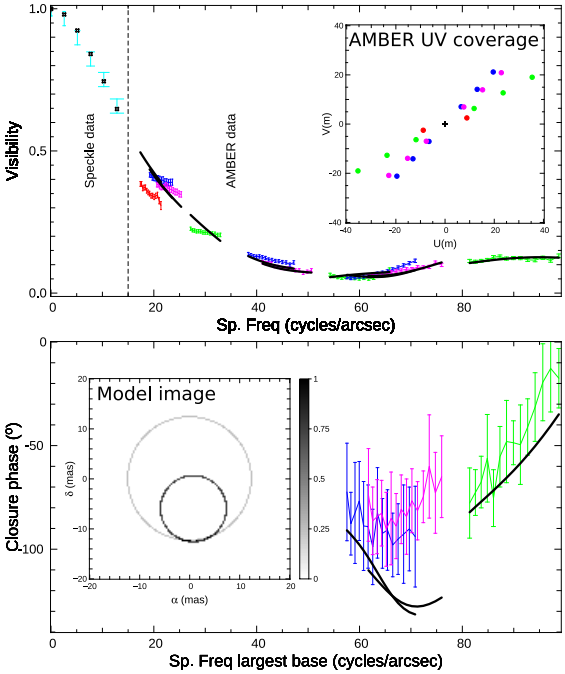

Fig. 1. AMBER visibilities (top, points with error bars, UV coverage in the inset) and closure phases (bottom) of WR 118, compared to the best-fitting model. The Yudin et al. (2001) data (light blue) are shown in the top panel. The best-fitting geometrical model made of two rings and an extended background component (40 mas FWHM, not sketched) is shown as black lines (model image in the inset of the bottom panel).

Parameter	Description	Value
S1	1^{st} ring size	24.8 ± 3.1 mas
F2	2^{nd} ring flux fraction	34 ± 7%
R. A.	2^{nd} ring R. A.-offset	0.79 ± 1.7 mas
Dec.	2^{nd} ring Dec.-offset	−6.0 ± 2.3 mas
S2	2^{nd} ring size	13.2 ± 1.0 mas
F3	Background flux fraction	46 ± 11%

Table 2. Parameters of our best-fitting geometrical model composed of two rings and an extended background component.

The reduced χ^2 of the solution was typically 50 depending on the models we tried to fit to the AMBER data. Therefore, all these models are probably an inappropriate representation of the measured visibilities and phases. Thus, in the next modeling step, we tentatively added a new, fully resolved component that dilutes the flux of the whole system. By including this additional fully resolved component, the reduced χ^2 for each model was considerably decreased (down to about 20). The results of our fitting procedure can be summarized as follows:

It is not possible to find a reasonable fit to the data with only a two-component model. A significant improvement of the fit is achieved by adding a fully resolved background component to the two-component models, accounting for $\approx$ 50% of the total flux. Thus, WR 118, as seen by AMBER, is composed of at least a fully resolved structure plus a component with a more complex shape, at smaller scales.

All the models have a typical size of $\approx$20 mas, which is approximately in agreement with the results of Yudin et al. (2001) and Monnier et al. (2007).

The models containing an extended component plus a point source locate the point source inside the extension of the resolved component. If this point source was a star and the resolved component a dust shell, then the putative companion star would be located inside the dust shell. Then, the companion star would have probably carved out the dust shell. Therefore, the hypothesis of having a continuous dust shell plus a well-separated companion can be discarded.

Our best-fitting model, which is able to reproduce both the visibilities and closure phases, consists of a set of two rings, with the smaller one located inside the larger one and with a contact zone in the South (see Table 2 and Fig. 1). Best-fitting models using more than two rings also show interweaved rings of increasing sizes.

Next, we provide a physical interpretation to describe the WR118 AMBER data, taking into account the knowledge acquired from the simple geometrical models.

3.2. Pinwheel model

Tuthill et al. (1999) and Monnier et al. (1999, 2007) showed that the dusty WR stars WR 98a and WR 104 are surrounded by spiral-like dusty nebulae. In particular, they found that the dust plume around these stars follow an Archimedian spiral, projected onto the plane of sky. Harries et al. (2004) presented a radiative transfer model of a bow-shock cavity between the winds of the two stellar components and successfully compared it with the observations.

The goal of this section is to demonstrate that a pinwheel nebula is consistent with all the features seen in the AMBER data of WR 118. To explain these features, we developed a geometrical model of a pinwheel nebula, based on the same simple geometrical models presented in the previous section. It is generated by adding many shifted elliptical rings of increasing sizes representing the bow-shock cavities at different orbital phases of the binary star along an Archimedian spiral, and then subsequently projecting them onto the plane of sky, as illustrated in the top panel of Fig. 2. Such a pinwheel model can be fully described by the following eight parameters:

- the extension S, and the number of turns T of the spiral,
- the size of the last ring s, corresponding to the opening angle $\theta = \arctan[s/S]$ of the wind-wind collision zone,
- the flux fraction f of the last ring relative to the central one; the ring flux in the spiral linearly decreases from 1 to f,

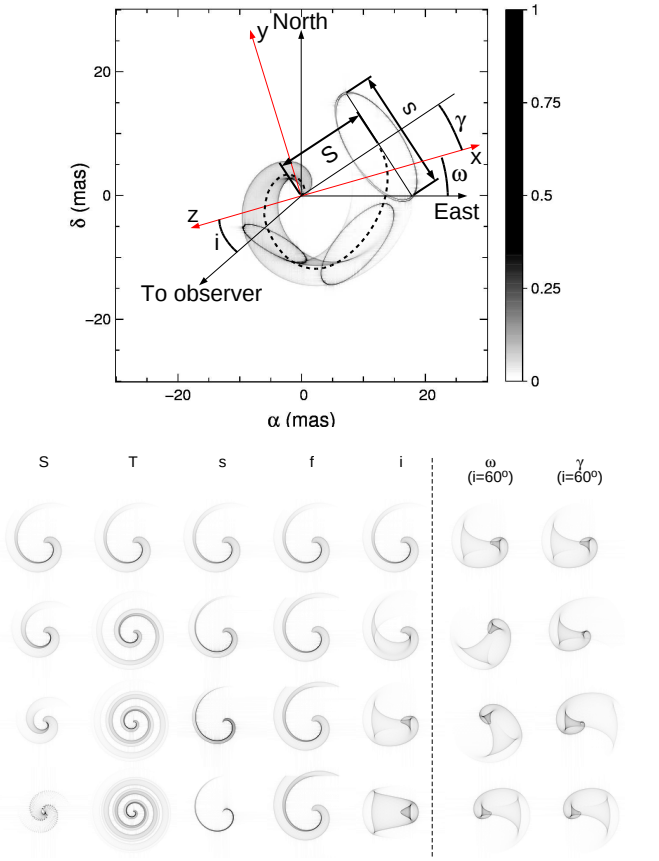

Fig. 2. Top: Sketch of our pinwheel nebula model. A series of elliptical rings (three of them are highlighted) following a projected Archimedian spiral (dashed line) set it up. The parameters of the model are labeled in the sketch. Bottom: Dependence of the pinwheel model on its parameters. For the first five parameters, the same model is shown in the first row. For the two last, a model with an inclination of 60° is shown.

- the three projection angles: i, ω and γ, to project the pinwheel on the plane of sky,
- F, the fractional flux of a fully resolved background.

To illustrate the meaning of the individual input parameters, in the bottom panel of Fig. 2, we show how the morphology of the pinwheel changes if a specific parameter is changed.

Following the results of Tuthill et al. (2008), who showed that for WR 104, the pinwheel flux sharply drops after exactly one turn around the binary star, we decided to fix $T = 1$ and $f = 0$ (see Table 3). Therefore, for our pinwheel model, we use the same number of free parameters (i.e. six) as in Sect. 3.1.

The best-fitting pinwheel model parameters are summarized in Table 3, and the comparison with the AMBER data is shown in Fig. 3. The qualitative agreement of the fit is very similar to the two-ring model described in the previous section, and the reduced χ^2 is also similar ($\chi^2 = 16$). Nevertheless, such a pinwheel model is much easier to understand from a physical point-of-view, for instance, in terms of a dust-emission signature in the wind-wind curved shock around a binary star.

Some parameters are well-constrained by our fit, such as the total extension of the pinwheel $S = 13.9 \pm 1.1$ mas, the extension of the extreme ring $s = 22.6 \pm 4.7$ mas, or the background flux contribution $F = 49 \pm 5\%$. On the other hand, other parameters like the projection angles onto the plane of sky and especially the inclination angle are poorely constrained. This may come from the tight range of position angles of the AMBER data.

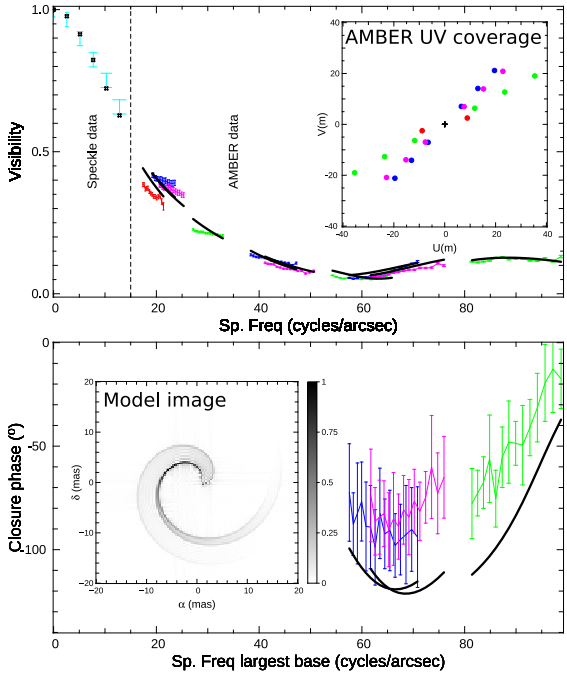

Fig. 3. Same as Fig. 1, but showing the best-fitting pinwheel model (black solid lines). An image of our best-fitting pinwheel model is shown in the bottom panel's inset.

Parameter	Description	Value
S	Total size	13.9 ± 1.1 mas
T	Turns	1 (fixed)
s	Ring-size at extremity	22.6 ± 4.7 mas
f	Flux at extremity	0 (fixed)
i	Inclination angle	3 ± 26°
ω	Orientation on sky	9.2 ± 9.6°
γ	Rotation angle	0.0 ± 9.6°
F	Background flux fraction	49 ± 5%

Table 3. Parameter of our best-fitting pinwheel model (see also Fig. 3).

We also found good agreement between our models and both the AMBER and Yudin et al. (2001) data sets by using a size for the extended component of ≈ 40 mas (see Figs. 1 and 3), which is fully resolved by AMBER.

3.3. Spherical wind clumping model

A second physical hypothesis to form dust in WR stars is wind clumping in single star winds (Cherchneff et al. 2000). We simulated a spherical clumped envelope by randomly putting unresolved "clumps" along a Gaussian profile with ≈ 30 mas FWHM. If we assume a small number of clumps (≤ 10), the model visibilities hardly match the observed ones, while some clump configurations match the observed closure phases. For many clumps (≈ 1000, hypothesis favored by, e.g., Lépine et al. 2000), the model visibilities more easily match the AMBER ones, while, on average, the model closure phases show values closer to zero (or 180°) than the observations.

Thus, from this study we qualitatively conclude that spherical wind-clumping models difficultly account for both the AMBER visibilities and closure phases.

4. Discussion and conclusion

Our study showed that our WR 118 data can be described by a dusty pinwheel nebula model. Other types of models describe the data equally well, but spherical wind-clumping models cannot easily explain both the observed visibilities and closure phases. Therefore, we suggest that WR118 is a binary star embedded in a pinwheel-like dust nebula.

Assuming the pinwheel hypothesis, we can measure the opening angle of the bow-shock of WR118: $\theta = \arctan[s/S] = 58 \pm 7°$. This is comparable to 40° in the case of WR104 (Tuthill et al. 2008). We also infer a period for the putative binary system in WR 118, assuming, like in WR 98a (Monnier et al. 1999), tidal circularization of the orbit. Given a typical wind terminal velocity of a WC9 star of 1200 kms^{-1} (Crowther 2007), a distance of ≈3 kpc for WR 118 (van der Hucht 2001), and an extension of 13.9 mas, the free-flying time of a dust plume from the center of the system to its farthest elongation is ≈60 days, corresponding to one full rotation of the binary in our model.

Such a period is remarkably shorter than the periods of 241.5 days for WR 104 (Tuthill et al. 2008), 565 days for WR 98a (Monnier et al. 1999) and 24.8 yrs for WR 112 (Marchenko et al. 2002). This would make WR 118 the shortest-period pinwheel system known today.

The short period found for WR 118 may also be compared to other known WR binaries. For instance, γ^2 Velorum is a WC8+O star with a similar period, of 78 days (Millour et al. 2007), but it does not produce dust. WR118 has a later spectral type than γ^2 Velorum, which alters the chemistry of the wind. Alternatively, the distance of WR 118 might be severely underestimated or its terminal velocity might be slower than for a typical WC9 star.

With the study presented in this paper, we demonstrated the potential of infrared long-baseline interferometry to resolve pinwheel nebulae around dusty WR stars. In van der Hucht (2001, 2006), we can find 24 permanent dust-producing WR stars, of which five (not yet including WR 118) have been confirmed to be colliding-wind binaries through the direct detection of pinwheel nebulae. Eight have near-infrared sizes strongly in favor of pinwheel nebulae (Tuthill et al. 2006; Monnier et al. 2007) and are just waiting to be confirmed. In total, there are 18 dusty WR stars still to be resolved by long-baseline interferometry in order to provide observational evidence that all WR permanent dust-maker are colliding winds binaries.

Acknowledgements. We thank the ESO VLTI team on Paranal and in Garching for carrying out the AMBER observations presented in this paper. The data were reduced using the publicly available data reduction software package *amdlib*, kindly provided by the Jean-Marie Mariotti Center (`http://www.jmmc.fr`).

References

Allen, D. A., Swings, J. P., & Harvey, P. M. 1972, A&A, 20, 333
Cherchneff, I., Le Teuff, Y., Williams, P., & Tielens, A. 2000, A&A, 357, 572
Chiar, J. E., Peeters, E., & Tielens, A. 2002, ApJ, 579, L91
Crowther, P. 2007, ARA&A, 45, 177
Crowther, P., Hadfield, L., Clark, J., Negueruela, I., & Vacca, W. 2006, MNRAS, 372, 1407
Harries, T., Monnier, J., Symington, N., & Kurosawa, R. 2004, MNRAS, 350, 565
Lépine, S., Moffat, A. F. J., St-Louis, N., et al. 2000, AJ, 120, 3201
Marchenko, S., Moffat, A., Vacca, W., Côté, S., & Doyon, R. 2002, ApJ, 565, L59
Millour, F., Chesneau, O., Borges Fernandes, M., et al. 2009, A&A, accepted.
Millour, F., Petrov, R. G., Chesneau, O., et al. 2007, A&A, 464, 107
Monnier, J., Tuthill, P., & Danchi, W. 1999, ApJ, 525, L97
Monnier, J., Tuthill, P., Danchi, W., Murphy, N., & Harries, T. 2007, ApJ, 655, 1033
Petrov, R. G., Malbet, F., Weigelt, G., et al. 2007, A&A, 464, 1
Richichi, A., Percheron, I., & Khristoforova, M. 2005, A&A, 431, 773
Tatulli, E., Millour, F., Chelli, A., et al. 2007, A&A, 464, 29
Tuthill, P., Monnier, J., & Danchi, W. 1999, Nature, 398, 487

Tuthill, P., Monnier, J., Tanner, A., et al. 2006, Science, 313, 935
Tuthill, P., Monnier, J. D., Lawrance, N., et al. 2008, ApJ, 675, 698
van der Hucht, K. A. 2001, New Astronomy Review, 45, 135
van der Hucht, K. A. 2006, A&A, 458, 453
Weigelt, G., Kraus, S., Driebe, T., et al. 2007, A&A, 464, 87
Williams, M. & van der Hucht, K. A. 1992, in A. S. P. Conf. Series, Vol. 22, 269
Williams, P. M. & van der Hucht, K. A. 2000, MNRAS, 314, 23
Williams, P. M., van der Hucht, K. A., & The, P. S. 1987, A&A, 182, 91
Yudin, B., Balega, Y., Blöcker, T., et al. 2001, A&A, 379, 229